



**HAL**  
open science

## Molecular interactions between tubulin tails and glutamylases reveal determinants of glutamylation patterns

Kathiresan Natarajan, Sudarshan Gadadhar, Judith Souphron, Maria M. Magiera, Carsten Janke

► **To cite this version:**

Kathiresan Natarajan, Sudarshan Gadadhar, Judith Souphron, Maria M. Magiera, Carsten Janke. Molecular interactions between tubulin tails and glutamylases reveal determinants of glutamylation patterns. *EMBO Reports*, 2017, 10.15252/embr.201643751 . hal-02376259

**HAL Id: hal-02376259**

**<https://hal.science/hal-02376259>**

Submitted on 22 Nov 2019

**HAL** is a multi-disciplinary open access archive for the deposit and dissemination of scientific research documents, whether they are published or not. The documents may come from teaching and research institutions in France or abroad, or from public or private research centers.

L'archive ouverte pluridisciplinaire **HAL**, est destinée au dépôt et à la diffusion de documents scientifiques de niveau recherche, publiés ou non, émanant des établissements d'enseignement et de recherche français ou étrangers, des laboratoires publics ou privés.

# Molecular interactions between tubulin tails and glutamylases reveal determinants of glutamylation patterns

Kathiresan Natarajan<sup>1,2,\*</sup> , Sudarshan Gadadhar<sup>1,2</sup>, Judith Souphron<sup>1,2,‡</sup>, Maria M Magiera<sup>1,2</sup> & Carsten Janke<sup>1,2,\*\*</sup> 

## Abstract

Posttranslational modifications of tubulin currently emerge as key regulators of microtubule functions. Polyglutamylation generates a variety of modification patterns that are essential for controlling microtubule functions in different cell types and organelles, and deregulation of these patterns has been linked to ciliopathies, cancer and neurodegeneration. How the different glutamylating enzymes determine precise modification patterns has so far remained elusive. Using computational modelling, molecular dynamics simulations and mutational analyses we now show how the carboxy-terminal tails of tubulin bind into the active sites of glutamylases. Our models suggest that the glutamylation sites on  $\alpha$ - and  $\beta$ -tubulins are determined by the positioning of the tails within the catalytic pocket. Moreover, we found that the binding modes of  $\alpha$ - and  $\beta$ -tubulin tails are highly similar, implying that most enzymes could potentially modify both,  $\alpha$ - and  $\beta$ -tubulin. This supports a model in which the binding of the enzymes to the entire microtubule lattice, but not the specificity of the C-terminal tubulin tails to their active sites, determines the catalytic specificities of glutamylases.

**Keywords** glutamylases; microtubules; molecular dynamics; TTLLs; tubulin code

**Subject Categories** Cell Adhesion, Polarity & Cytoskeleton; Post-translational Modifications, Proteolysis & Proteomics; Structural Biology

**DOI** 10.15252/embr.201643751 | Received 2 December 2016 | Revised 15 March 2017 | Accepted 22 March 2017 | Published online 8 May 2017

**EMBO Reports (2017) 18: 1013–1026**

## Introduction

Microtubules (MTs) are key cytoskeletal polymers in eukaryotes. They are essential for cell division, cell shape, motility,

intracellular transport and neuronal functions. An emerging mechanism to adapt MTs to this variety of functions is the tubulin code, which suggests that properties and functions of MTs could be modulated by the expression of alternative  $\alpha$ - and  $\beta$ -tubulin genes, and by the posttranslational modification (PTM) of tubulin dimers [1]. PTMs that take place on the carboxy-terminal tails of  $\alpha$ - and  $\beta$ -tubulin can control the functions of the modified MT by regulating the recruitment of MT-associated proteins (MAPs) and motors (reviewed in [2]). Two of these PTMs, polyglutamylation [3] and polyglycylation [4], catalyse the formation of secondary peptide chains at glutamate residues within the C-terminal tubulin tails. Due to their capacity to modify both  $\alpha$ - and  $\beta$ -tubulin, to generate branch-peptide chains of different length, and to use different modification sites within the  $\alpha$ - and  $\beta$ -tubulin tails, these PTMs generate highly complex modification patterns to fine-tune MT functions (reviewed in [2]). This concept was validated by a recent work showing how gradual variations of tubulin glutamylation levels act as a rheostat to regulate MT severing in a non-linear, biphasic manner [5].

To generate these complex patterns, the modifying enzymes require a strict control of their activity and specificity. Polyglutamylases and polyglycylation belong to the tubulin tyrosine ligase-like (TTLL) family [6–10], which in mammals comprises nine glutamylases, three glycylation and one tyrosine ligase, the founding member of the family [11]. Different glutamylases and glycylation generate glutamate or glycine chains of different lengths, might use different modification sites and have preferences for modifying either  $\alpha$ - or  $\beta$ -tubulin [7,8]. However, as the catalytic domain of all TTLLs is highly conserved, it has remained unclear how the enzymes control their different reaction preferences [7].

To answer this question, it is fundamental to determine the mode of interactions between the glutamylases and their substrates, the tubulin C-terminal tails. Strikingly, these tails have never been entirely visualized in structural studies. A partial density of the  $\alpha$ -tubulin tail has been seen in the crystal structure of TTL bound to

<sup>1</sup> Institut Curie, CNRS, UMR 3348, PSL Research University, Orsay, France

<sup>2</sup> CNRS, UMR 3348, Université Paris Sud, Université Paris-Saclay, Orsay, France

\*Corresponding author. Tel: +1 507 2845297; E-mail: natarajan.kathiresan@mayo.edu

\*\*Corresponding author. Tel: +33 169863127; E-mail: carsten.janke@curie.fr

<sup>†</sup>Present address: Physiology and Biomedical Engineering, Mayo Clinic, Rochester, MN, USA

<sup>‡</sup>Present address: Unité de Pathogénie Microbienne Moléculaire, INSERM U1202, Institut Pasteur, Paris, France

tubulin, but even in this structure, a large part of the tail was not well resolved [12]. In the first structure of a glutamylase bound to the MT lattice, which was obtained by an elegant combination of X-ray crystallography, high-resolution electron microscopy and molecular modelling, the tubulin tails were only partially seen [13]. It thus appears that direct structural data of the tubulin tails within the active site of TTLL glutamylases or glycyllases will be difficult to obtain, most likely due to intrinsically disordered nature and high flexibility of the tubulin tails [14], and the resulting dynamicity of their interactions with the modifying enzymes.

To overcome these limitations, we used molecular modelling and molecular dynamics (MD) simulations to determine the substrate recognition mode of glutamylases. We predicted key residues involved in catalysis and substrate binding of TTLL5, a glutamylase that preferentially modifies  $\alpha$ -tubulin, confirmed our model by structure-guided site-directed mutagenesis and activity assays, and compared it to TTLL7, a  $\beta$ -tubulin glutamylase. Our model strongly suggests that the mode by which the tubulin tail interacts with the catalytic pocket of TTLLs is compatible with the modification of both,  $\alpha$ - and  $\beta$ -tubulin. Moreover, due to the dynamics of these

interactions, multiple sites within the tubulin tails are accessible for glutamylation, however, with a clearly defined preferential site of modification. Our work provides a molecular framework for the mechanism of action of tubulin glutamylases that explains their mode of catalysis, thus providing insights into the signalling potential of the tubulin code.

## Results

### Homology modelling of TTLL enzymes

Based on the available crystal structures of tubulin tyrosine ligase TTL [12,15], and the glutamylase TTLL7 [13], we homology-modelled the structures of murine TTLL4, TTLL5, TTLL6 and TTLL7 to predict a conserved common scaffold. The conservation map of these four glutamylases shows that residues in the active site and around the ATP-binding site are highly conserved (Fig 1A). The structure-based sequence alignment shows that all four modelled TTLLs share a common structural fold (Fig EV1). Finally,

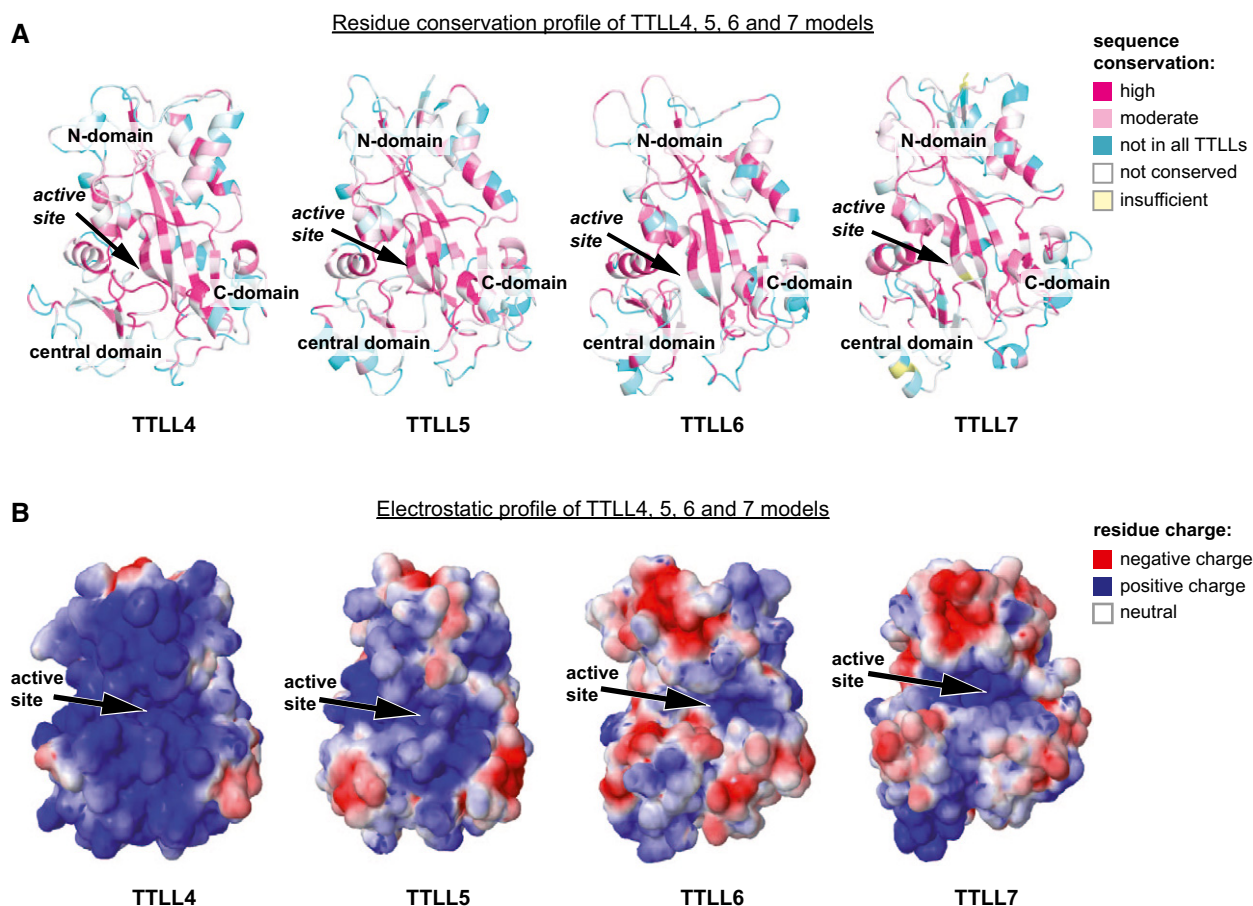


**Figure 1. Structural modelling and domain comparison between TTLLs.**

A Structural models (cartoon representation) of TTLL4, TTLL5, TTLL6 and TTLL7 core domains, generated from the structural alignment (Fig EV1) of the protein sequences. The conservation profile mapping [52] is colour-coded as indicated.

B Electrostatic-potential map (surface representation) of TTLL4, TTLL5, TTLL6 and TTLL7. Red patches denote negative charges, whereas blue patches denote positive charges and the white patches represent neutral. Note that in all TTLLs, the active site is positively charged.

electrostatic analysis revealed that active site is formed by a deep cavity lined by a stretch of positively charged residues (Fig 1B), allowing for interaction with their substrates, the negatively charged C-terminal tubulin tails. Considering the similarity of these sites raised the question of how different enzymes acquire their known reaction preferences [7]. Answering this question requires a structural view of the binding of these tails into the active site of the enzymes. We decided to simulate this binding for TLL5, an  $\alpha$ -tubulin-modifying glutamylase, and compare it to TLL7, an enzyme with a strong preference for  $\beta$ -tubulin.

### Structural dynamics of TLL5 upon $\alpha$ -tubulin tail binding

To understand how the tubulin C-terminal tails could influence the active site of polyglutamylases, we performed molecular dynamics (MD) simulations of ADP-bound TLL5 alone (apo-form), or with the C-terminal tail of  $\alpha$ 1-tubulin. The structural stability of the models was assessed by calculating time evolution of potential energy during simulations (Appendix Fig S1A and B) and the time-dependent changes in the root-mean-square deviation (RMSD) between TLL5 apo and  $\alpha$ -tubulin-tail-bound simulation of TLL5

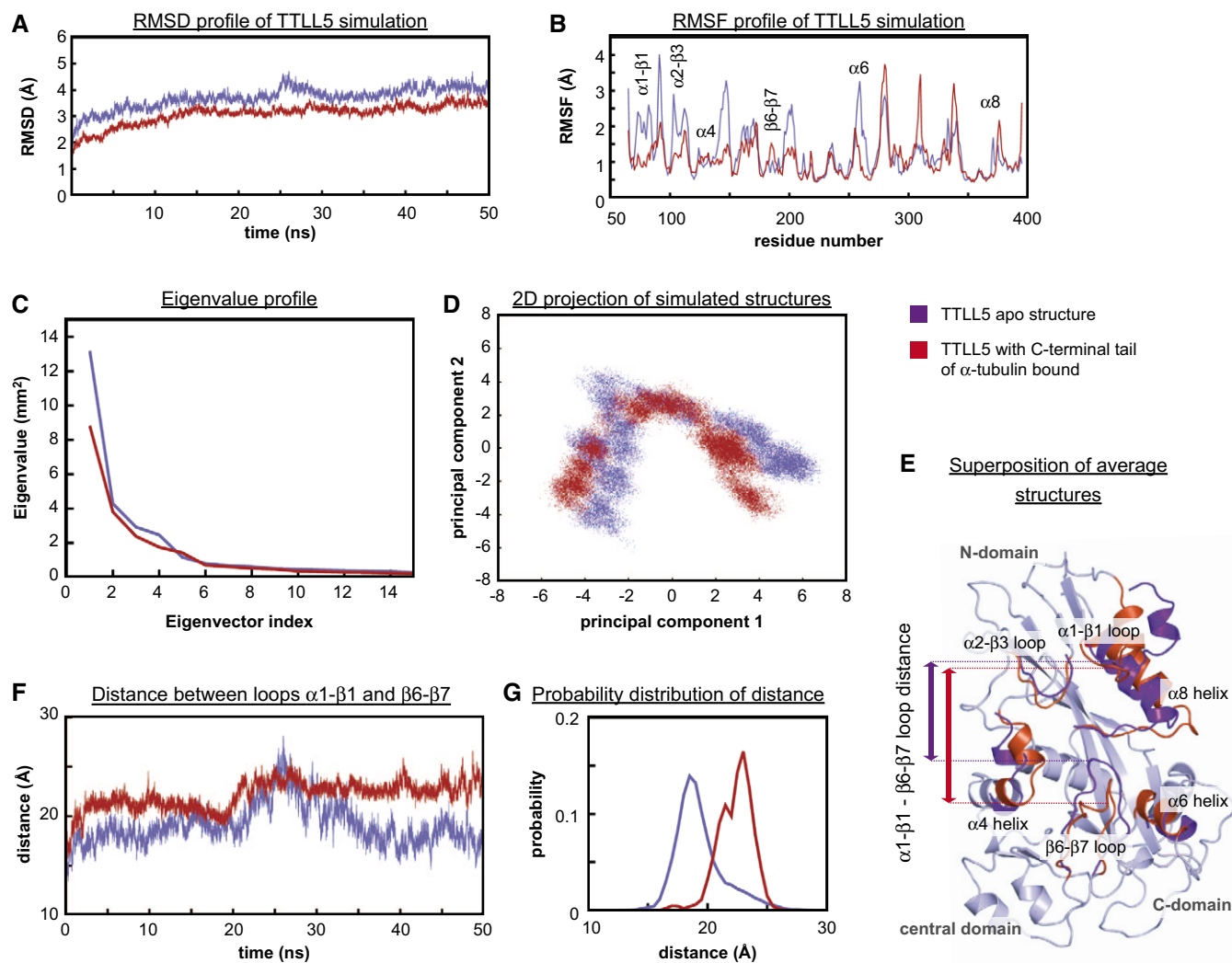


**Figure 2. Molecular dynamics analyses of TLL5.**

Molecular dynamics simulations of TLL5 in the apo- (purple) and the  $\alpha$ -tubulin-tail-bound (dark red) form.

- A Time evolution of RMSD values of backbone atoms from TLL5. The RMSD changes were calculated with respect to the equilibrated structure from apo- and tail-bound simulations.
- B RMSF values of C $\alpha$  atoms comparing apo- and tail-bound simulations.
- C Eigenvalue profile of the first 15 eigenvectors from TLL5-apo- and tail-bound simulations.
- D Two-dimensional projection of simulated structures from (C) TLL5 in the apo- and the  $\alpha$ -tubulin-tail-bound form onto the plane constituted by first two principal components.
- E Superposition of the time-averaged structural simulations (cartoon representation) of TLL5 in the apo- and  $\alpha$ -tubulin-tail-bound form. The secondary structural elements that underwent most significant conformational changes are highlighted.
- F Time evolution of distance between the centre of mass (COM) of the loops  $\alpha$ 1- $\beta$ 1 and  $\beta$ 6- $\beta$ 7.
- G Probability distribution plot of the distance between COM of the loops  $\alpha$ 1- $\beta$ 1 and  $\beta$ 6- $\beta$ 7.

(Fig 2A). In terms of RMSD values, the enzyme shows an overall stable structure, especially with the tubulin tail bound, in which the mean RMSD value is lower ( $3.081 \pm 0.39 \text{ \AA}$ ) as compared to the apo-form ( $3.699 \pm 0.40 \text{ \AA}$ ), indicating that TTLL5 moves into a more stable conformation upon binding of the tubulin tail. Furthermore, the stable time evolution of potential energy values also indicated that the systems have converged. The RMSD values were calculated from respective simulations with respect to the structure after equilibration. RMSD values indicate the structural deviations (changes in atomic positions) that occur during simulations compared to the starting structure of simulations. Our simulations clearly demonstrate that the TTLL5 core domain is stabilized upon  $\alpha$ -tubulin tail binding, as the TTLL5- $\alpha$ -tubulin-tail complex shows lower and more stable RMSD values during simulations as compared to apo-TTLL5. The convergence of simulations was also verified through calculating the root-mean-square inner product (RMSIP) overlap matrix for the first and second half of the trajectories from the simulations. The RMSIP overlap matrix showed overlap among several principal components, which further confirmed the convergence of simulations (Appendix Fig S2A and B).

To measure the dynamic changes that occur at the level of single residues, we calculated the root-mean-square fluctuations (RMSF), which represent the movement of each C $\alpha$  atom around its average position. RMSF values of TTLL5 with or without (apo) the  $\alpha$ -tubulin tail show a reduced dynamics of TTLL5 upon tubulin-tail binding (Fig 2B), indicating an overall compaction of the TTLL5 structure upon binding the  $\alpha$ -tubulin tail and ADP into the active site. A similar disorder-to-order transition was observed in crystal structures of TTL core domain, which has a partially disordered active site in the absence of the  $\alpha$ -tubulin tail [15], but becomes compact upon engaging  $\alpha$ -tubulin and ATP [12].

### TTLL5 remodels its active site upon binding of the $\alpha$ -tubulin tail

Our results predict that binding of the  $\alpha$ -tubulin tail into the active site of TTLL5 compacts the core domain of the enzyme. However, due to the high dimensionality of the protein dynamics, it is difficult to identify the dominant motions within the enzyme during simulation. We thus used principal component analysis (PCA) to locate the essential motions of TTLL5 during its transition from the apo- to the  $\alpha$ -tubulin-tail-bound form. All backbone atoms of the apo- and tubulin-tail-bound forms of the enzyme were included in the PCA analyses, which were performed separately for both systems. In these analyses, we determined the relative contribution of different movement modes (eigenvectors) to the overall motions of the TTLL5 core domain.

Our PCA clearly shows that the overall TTLL5 dynamics can be described by a small number of eigenvectors (Fig 2C). The first six eigenvectors mostly determine the total mean square fluctuations of the enzyme dynamics. The presence of the  $\alpha$ -tubulin tail in the active site restricts the dynamics of TTLL5 core domain to lower eigenvalues. Plotting the two-dimensional projections of MD structures on the plane defined by the first two eigenvectors reveals strong differences in fluctuation between apo- and tail-bound forms of TTLL5 (Fig 2D). As the principal components shown in Fig 2D are projected onto identical eigenmodes, they can be directly compared. The presence of the  $\alpha$ -tubulin tail in the active site restricts the dynamics of TTLL5, resulting in a coupling of the first

two eigenvectors, which is not the case in the apo-form of TTLL5. This indicates a cooperative mechanism of tubulin-tail binding. To visualize this, we superimposed the average structures of TTLL5 simulations in the apo- and the  $\alpha$ -tubulin-tail-bound form. This demonstrated that a number of structural elements of TTLL5 undergo significant rearrangements during simulations, such as the N-domain-loops  $\alpha$ 1- $\beta$ 1 (71–80),  $\alpha$ 2- $\beta$ 3 (101–107), helix  $\alpha$ 8 (378–391), central-domain loop  $\beta$ 6- $\beta$ 7 (178–192) and the C-domain helix  $\alpha$ 6 (269–278) (Fig 2E).

As the TTLL5-apo simulation showed that the active site opens and closes spontaneously, we have calculated the distance between the centre of the mass (COM) of the loops  $\alpha$ 1- $\beta$ 1 located in the N-terminal domain, and  $\beta$ 6- $\beta$ 7 in the C-terminal domain. The  $\beta$ 6- $\beta$ 7 loop shows the strongest oscillations of all structural elements (Fig 2E). Upon binding of the  $\alpha$ -tubulin tail, however, the loop adapts a stable open conformation, which fixes the tail into the active site (Fig 2F). This behaviour is reflected in the probability distribution of COM distance between the loops  $\alpha$ 1- $\beta$ 1 and  $\beta$ 6- $\beta$ 7, which is overall greater in the presence of the C-terminal tail of  $\alpha$ -tubulin in the active site of TTLL5 (Fig 2G). It is likely that the electrostatic interactions between negatively charged  $\alpha$ -tubulin tail and the positively charged  $\beta$ 6- $\beta$ 7 loop play a role in maintaining the  $\beta$ 6- $\beta$ 7 loop in this open state.

Our simulations strongly suggest that opening of the  $\beta$ 6- $\beta$ 7 loop is required to orient and accommodate the  $\alpha$ -tubulin tail into the active site of the enzyme. The intrinsic flexibility of this region also explains why the  $\beta$ 6- $\beta$ 7 loop was not fully resolved in the crystal structures of both, TTLL7 and TTL [12,13,15]. The importance of the  $\beta$ 6- $\beta$ 7 loop is further underpinned by our observations that either deleting or exchanging this loop for the corresponding sequence of TTLL6 results in loss of activity of TTLL5 (see below; Fig 4).

### Determination of the molecular components involved in the binding of the $\alpha$ -tubulin tail

The  $\alpha$ -tubulin tail binds to the conserved patch of positive residues located in the centre of the TTL core domain. Plotting the binding modes of the tail and TTLL5 along the first principal component axis reveals concerted movements of the structural elements of TTLL5 and the  $\alpha$ -tubulin tail (Fig EV2A). The inter-molecular interactions after 50 ns simulation show that the  $\alpha$ -tubulin tail is stabilized by several salt-bridges, hydrogen bonds and non-bonded contacts with a number of conserved residues in the active site of TTLL5 (Figs 3A and EV3A).

To measure the impact of single binding determinants of the TTLL5- $\alpha$ -tubulin-tail interactions, we calculated the percentage of hydrogen bonding occupancy of interacting residues (Appendix Table S1) using the H-bond tool of the Visual Molecular Dynamics (VMD) software [16]. In our analysis, the terminal residues of the  $\alpha$ -tubulin tail (449–451) have the strongest H-bonding occupancies. E445 forms a salt-bridge interaction with R188 of the  $\beta$ 6- $\beta$ 7 loop of TTLL5, thus orienting E445 towards the ATP/ADP-binding site. This implies that E445 might be the preferential residue to be glutamylated (Fig 3A). Nevertheless, the intrinsically disordered nature of the tubulin tail [14] and its conformational flexibility within the active site (Fig EV2A) might allow for the modification of other glutamate residues within the  $\alpha$ -tubulin tail. Calculation of RMSF values of all  $\alpha$ -tubulin-tail residues within the active site further

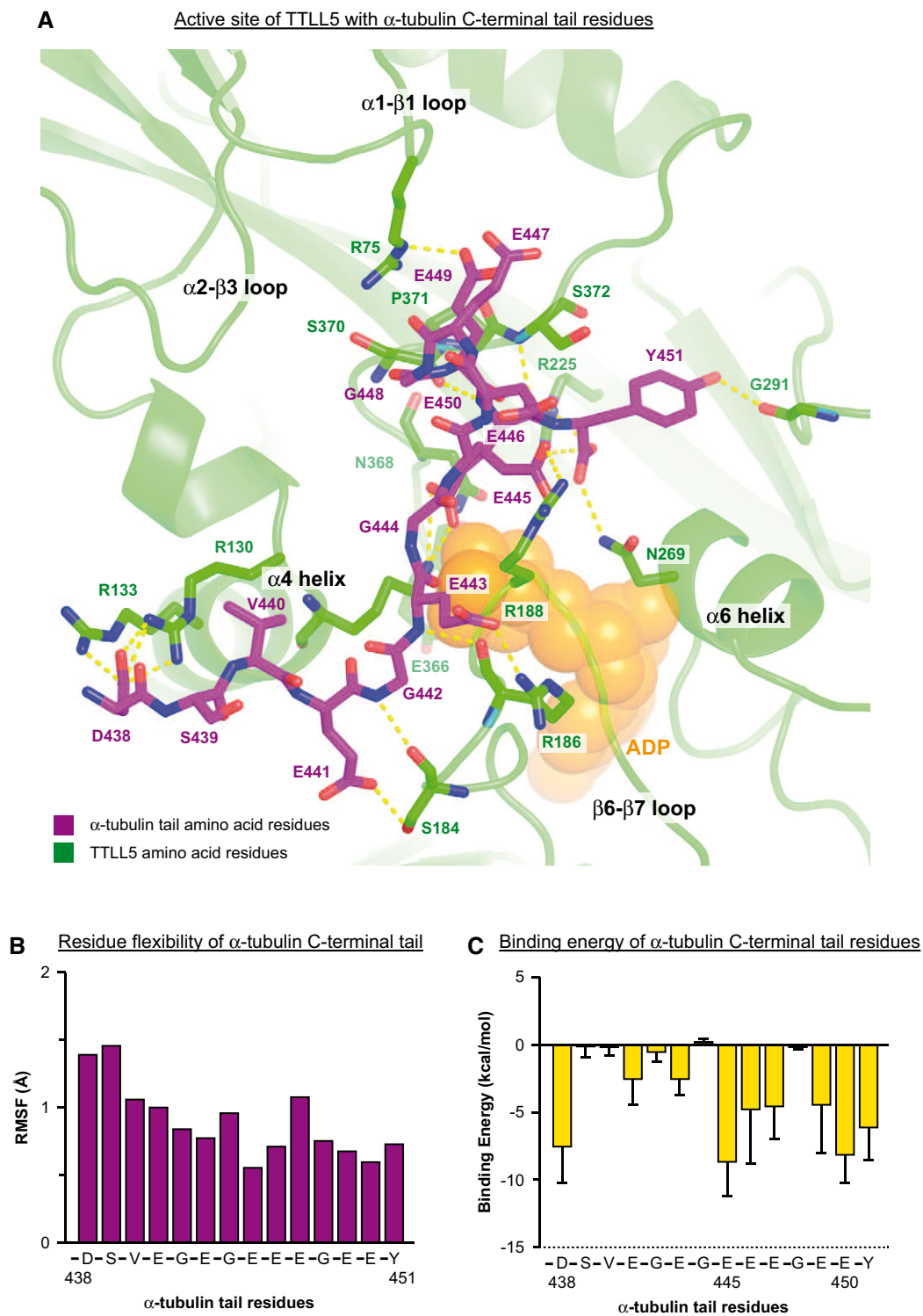


**Figure 3. Docking of the  $\alpha$ -tubulin tail into TLL5.**

A Predicted residue interactions between the residues of  $\alpha$ -tubulin tail (purple) and of the active site of TLL5 (green). The dotted yellow lines denote the hydrogen bonding interactions.

B RMSF values of the C $\alpha$  atoms of  $\alpha$ -tubulin-tail residues bound to the active site of TLL5 during simulations.

C The binding energy values ( $\Delta G$ ) for  $\alpha$ -tubulin-tail residues bound to TLL5 calculated at 5-ns intervals using the ANCHOR web server [53]. Error bars indicate the standard deviation between 10 iterations taken at the 5-ns intervals.

confirmed the lower structural flexibility of the C-terminal part of the tail (Fig 3B). While the N-terminal part of the tail shows more freedom of movement in our simulations, it will certainly be constrained in the context of the entire tubulin molecule, where this part is connected to the tubulin body.

The binding energy values for  $\alpha$ -tubulin-tail residues were calculated through the ANCHOR web server, which determines changes in solvent-accessible surface areas for the interface residues and estimates their contribution to the binding free energy. The binding energy of each contacting residue was then calculated with FastContact [17], which uses a distance-dependent dielectric electrostatic and desolvation contact potential [18]. The binding energy analyses strongly suggest that the tubulin tail is anchored into the active site of TLL5 through residues D438, E445 and E450 (Fig 3C), suggesting that these residues stabilize the  $\alpha$ -tubulin tail in the active site. To visualize the structural changes in the  $\alpha$ -tubulin tail in the active-site environment, we determined the time evolution of RMSD and radius of gyration values for the  $\alpha$ -tubulin tail. The  $\alpha$ -tubulin tail showed a mean RMSD value of  $1.993 \pm 0.39 \text{ \AA}$  and a mean radius of gyration value around  $0.889 \pm 0.045 \text{ nm}^2$  in the active site during simulations. The radius of gyration value is indicative of the compactness of a protein or peptide structure during simulations. Both time evolution of the RMSD (Appendix Fig S3A) and the radiation of gyration values (Appendix Fig S3B) show that the  $\alpha$ -tubulin tail stabilizes and achieves compact conformation in the active site after 20 ns. The secondary-structure analysis further shows that the intermediate residues 445–448 form a stable turn conformation into the active site of TLL5 (Fig EV3B). Thus, the intrinsically disordered  $\alpha$ -tubulin tail is restructured in the active-site environment, which favours an induced-fit model of enzyme dynamics.

#### Mutational analysis of TLL5 validates its $\alpha$ -tubulin-tail binding mode

To confirm the results of our simulations, and determine the key residues required for enzymatic activity, we performed structure-guided mutagenesis of TLL5. We selected residues involved in the interaction of active site of TLL5 with the tubulin tail, as well as residues involved in ATP/ADP binding (Fig 4A) for mutagenesis. In addition, we investigated the role of the  $\beta$ 6- $\beta$ 7 loop, which shows a

similar conformation in the models of TLL4, TLL5 and TLL7, but is differently arranged in the TLL6 model (Fig 4B). This loop sterically restricts the binding pocket of the tubulin tails and might thus be important for enzymatic activity.

The mouse TLL5 gene fused to EYFP [7] was mutated with primer pairs containing single point mutations. To delete or replace the  $\beta$ 6- $\beta$ 7 loop (Fig 4C), a ligation-independent cloning strategy was employed [19]. The proteins were expressed in HEK293T cells, collected after 20 h, and lysates were separated on SDS-PAGE and immuno-blotted with antibodies for glutamylation (GT335) and polyglutamylation (polyE) [20]. Tubulin load (12G10) and expression of TLL5-EYFP variants were verified (Fig 4D). In contrast to untransfected controls, a clear GT335 labelling of  $\alpha$ -tubulin, and to a lower extent  $\beta$ -tubulin, was found after expression of wild-type TLL5. Some higher-molecular-weight bands, which represent non-tubulin substrates of TLL5, were also detected [21]. Comparing wild-type TLL5 with mutated variants showed that some of the mutated forms of TLL5 were fully active, while others showed reduced activity, and some were completely inactive. This result was confirmed with the polyE antibody (Fig 4D).

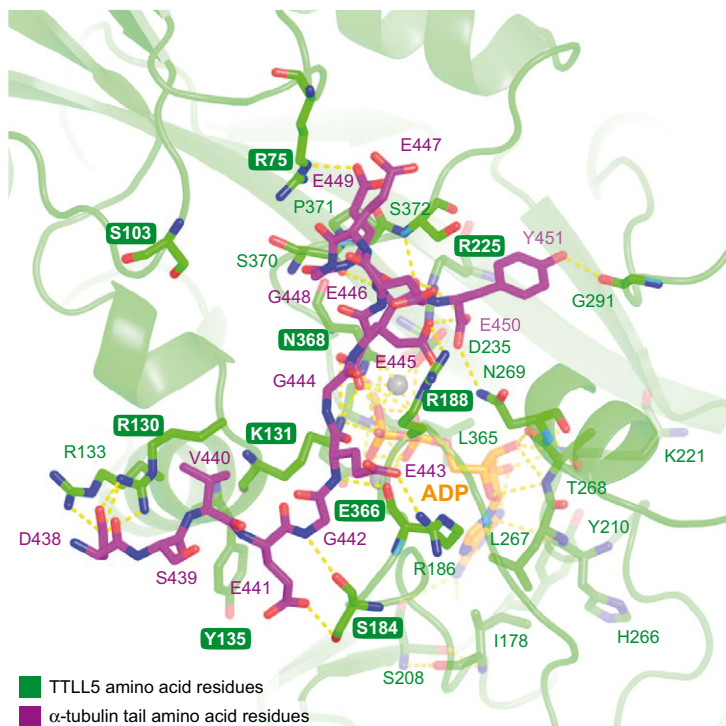
We further confirmed the results of the immunoblots using the extracts from HEK293T cells expressing TLL5-EYFP variants in an *in vitro* glutamylase activity assay. The test was performed with three biological replicates (i.e. three independent transfections of HEK293T cells with the series of expression plasmids, followed by the enzymatic assay for each cell extract). The incorporation of [ $^3\text{H}$ ]-glutamate into  $\alpha$ -tubulin (Fig 4E) provides values of enzymatic activity of the different TLL5 variants, which fully confirmed the observations of the immunoblots (Fig 4D). In contrast to  $\alpha$ -tubulin, which was clearly modified by the active TLL5 variants,  $\beta$ -tubulin modification showed no significant differences from the intrinsic polyglutamylase activity of the HEK293T cells (Fig EV4). This confirms that under non-saturating conditions, TLL5 acts exclusively as an  $\alpha$ -tubulin-specific glutamylase (Fig 4D) [7].

Both immunoblot analyses and the glutamylation activity assay coherently showed that mutation of residues R225, N368, E366 and K131 abolishes the enzymatic activity of TLL5. These results confirm our modelling and MD simulations, which had suggested that R225 interacts with the carboxyl group of E450 of the  $\alpha$ -tubulin tail by stabilizing the C-terminal part of the tail inside the active site. Similarly, N368 interacts with the side chain of  $\alpha$ -tubulin E450, thus

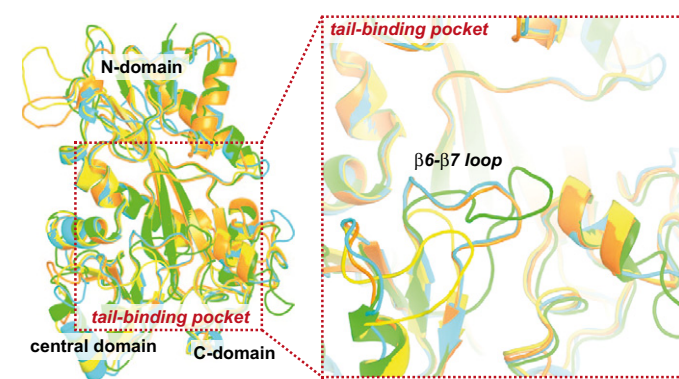
#### Figure 4. Mutational analyses of TLL5 residues important for catalysis of glutamylation.

- Binding mode of the  $\alpha$ -tubulin tail and ADP in the TLL5 active site after 50 ns of simulation. The interactions between  $\alpha$ -tubulin tail (purple), ADP (orange) and TLL5 residues (sticks, green) are shown. The key residues selected for site-directed mutagenesis are highlighted in green boxes. The  $\text{Mg}^{2+}$  ion is shown as grey sphere. The dotted yellow lines denote the hydrogen bonding interactions.
- Superposition of structural models (Fig 1A) of the core domains of TLL4 (orange), TLL5 (green), TLL6 (yellow) and TLL7 (cyan), with a detailed view of the  $\beta$ 6- $\beta$ 7 loop.
- Sequence alignment of TLL4, TLL5, TLL6 and TLL7 using Clustal X software [54] showing the peptide sequences of the  $\beta$ 6- $\beta$ 7 loop. The sequence of the loop of TLL5 was either deleted ( $\Delta$ 1-loop) or replaced by the sequence of TLL6 ( $\Delta$ 2-loop).
- Immunoblot analysis of HEK293T cell extracts expressing different forms of TLL5-YFP. The presence or absence of glutamylase activity was determined with the glutamylation-specific antibodies: GT335 and polyE [20]. Equal tubulin loads were controlled with the anti- $\alpha$ -tubulin antibody 12G10 and TLL5-YFP expression with an anti-TLL5 serum.
- In vitro* glutamylase activity assay: HEK293T cells expressing different TLL5 versions and non-transfected controls were lysed and incubated with [ $^3\text{H}$ ]-glutamate and purified MTs.  $\alpha$ -tubulin-glutamylase activity was determined by measuring the radioactivity of the  $\alpha$ -tubulin protein bands. The mean values with standard deviation for three biological replicates are plotted. The grey dashed line indicates the basal activity of extracts from non-transfected HEK293T cells. For  $\beta$ -tubulin, see Fig EV4.
- Structural model of TLL5 (surface representation) with the positions of the experimentally tested interaction sites for the  $\alpha$ -tubulin tail. The colours of the residues represent the experimentally determined role in the catalytic process. Red amino acids are essential—their mutation leads to complete loss of activity, purple are involved in the catalytic process, and their mutations lead to reduced activity, whereas blue residues did not visibly affect the activity of the enzyme upon mutation.

**A** Active site of TTLL5 with  $\alpha$ -tubulin C-terminal tail residues



**B** Position of the  $\beta$ 6- $\beta$ 7 loop in the tail-binding pocket

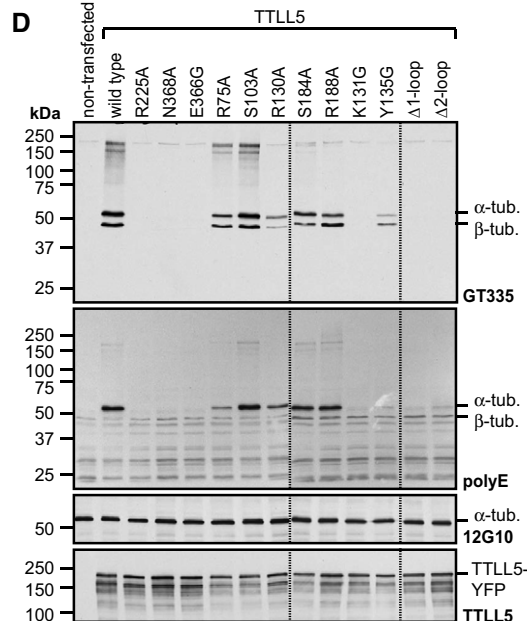


**C** Sequence alignment and mutagenesis of the  $\beta$ 6- $\beta$ 7 loop

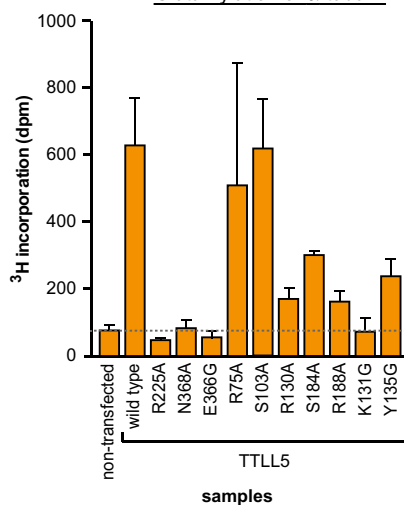
TTLL4	618	QDSKLLR---KATNESSSRQKNIIVKPPASARGIGTQVTHKWS
TTLL5	161	AEYAEPFC---NSYSRD-RGPWIVVKPVASSRGRGVYLLINNP
TTLL6	154	ADWCDLQ---TYSRTRKKNKTYICKPDSGCQGRGIFTRSVK
TTLL7	136	SEYTFQPNVYKELKKRKKOKTRIVKPNAGAMCHGISLIRNGD

TTLL5- $\Delta$ 1-loop: deletion of VASSRGRG

TTLL5- $\Delta$ 2-loop: replacement VASSRGRG with DSGCQGRG



**E** Glutamylation of  $\alpha$ -tubulin



**F** TTLL5 structural model with interaction sites important for enzymatic activity

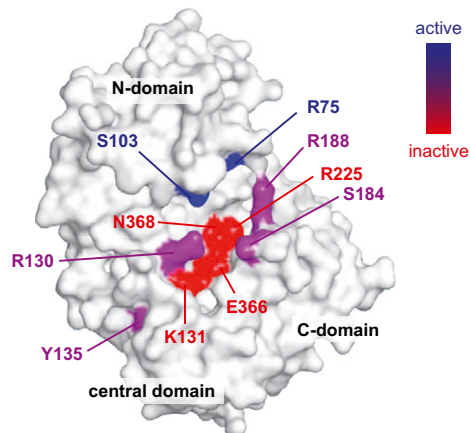


Figure 4.

stabilizing the tail in the catalytic pocket. At the same time, N368 also mediates interaction with ADP/ATP, and residues E366 and K131 directly interact with ADP/ATP and stabilize the nucleotide into its binding groove (Fig 4A). E366 is highly conserved in all TTLLs, and its mutation to glycine has coherently led to the loss of enzymatic activity [7,8].

Mutations of R130, S184, R188 and Y135 lead to a reduced enzymatic activity of TTLL5. In our simulations (Fig 2), these four residues are involved in the stabilization of the tubulin tail in the active site; thus, a reduced enzymatic activity upon their mutation was expected. R130 is located at the entrance of the tail-binding pocket in  $\alpha$ -helix 4 of the enzyme and makes contacts with D438 and S439 of the  $\alpha$ -tubulin tail, thus stabilizing the N-terminal part of the tail. Residues S184 and R188 are located in the  $\beta$ 6- $\beta$ 7 loop and interact with glutamate residues in the  $\alpha$ -tubulin tail. The movement of  $\beta$ 6- $\beta$ 7 loop during simulations and the location of these residues in the structural model tempt us to suggest that they might help to orient E435 towards the active site. Mutation of Y135, which is located at the base of the helix  $\alpha$ 4 below the entrance of the tail-binding pocket, could indirectly affect the contacts between tubulin tail and enzyme, or might affect the conformation of the helix, thus affecting enzyme activity.

Mutation of R75 and S103, two residues located in the  $\alpha$ 1- $\beta$ 1 and  $\alpha$ 2- $\beta$ 3 loops, did not visibly affect the glutamylating activity of TTLL5. In the simulation, these regions undergo significant changes upon tail binding (Fig 2). While this suggests that they are not directly involved in regulating the activity of the enzyme, they might stabilize the tubulin tail once the glutamylation reaction is initiated and glutamate chains are elongated.

Finally, our models show that the loop  $\beta$ 6- $\beta$ 7 restricts the active site of all TTLL polyglutamylases (Fig 4B), but its peptide sequence is not conserved (Fig 4C). Deletion of this loop (TTLL5- $\Delta$ 1-loop; Fig 4C) led to a complete loss of enzymatic activity (Fig 4D). As the deletion of eight amino acids could induce long-range structural alterations, we next replaced the loop with the complementary sequence of TTLL6 (TTLL5- $\Delta$ 2-loop; Fig 4C). Again, TTLL5- $\Delta$ 2-loop was inactive (Fig 4D), indicating that the  $\beta$ 6- $\beta$ 7 loop, despite its lack of amino acid conservation between different TTLLs and despite its conformational flexibility, plays a key role in the catalysis of glutamylation.

Based on our mutation analysis, we generated a structural view of TTLL5 (Fig 4F), which reveals the presence of an essential core domain (red) in which mutations of single amino acid residues lead to the complete loss of enzymatic activity. This region is surrounded by a larger domain (purple), in which mutations lead to decreased glutamylation activity, whereas residues further away from these two domains (blue) do not visibly influence the enzymatic activity of TTLL5.

### Structural dynamics of $\beta$ -tubulin tail binding into TTLL7

To compare the mode of binding of  $\alpha$ - and  $\beta$ -tubulin tails into the active sites of TTLL polyglutamylases, we docked the C-terminal tail of  $\beta$ 2-tubulin into the active site of TTLL7 and performed simulations of TTLL7 in the tail-bound and tail-unbound (apo-) forms. Similar to TTLL5 simulations (Fig 2), the TTLL7 core domain is stabilized upon  $\beta$ -tubulin tail binding, as the TTLL7- $\beta$ -tubulin-tail complex shows lower RMSD values during simulations as compared to apo-TTLL7 (Fig 5A). This confirms that similar to TTLL5, the active site of TTLL7 is remodelled upon substrate binding. The RMSF values of TTLL7 also show a reduced dynamics upon binding of the  $\beta$ -tubulin tail (Fig 5B), which is similar to TTLL5 as well (Fig 2B). The structural stability of the models was tested by calculating time evolution of potential energy during simulations (Appendix Fig S1C and D), and the convergence of simulations was confirmed by the RMSIP overlap matrix (Appendix Fig S2C and D).

In our simulation, the  $\beta$ -tubulin tail binds to the active site of TTLL7 through a stretch of glutamate residues. This is very similar to the mode by which the  $\alpha$ -tubulin tail binds to TTLL5; however, the  $\beta$ -tubulin tail is more stretched, and the very C-terminal residues project out of the active site (Fig 5C). This is reflected in the time evolution of RMSD and radius of gyration values during simulation. Both values increase in the course of simulations (Appendix Fig S3C and D), which is not the case in the simulation of the  $\alpha$ -tubulin tail binding to TTLL5 (Appendix Fig S3A and B). The observation that the very C-terminal portion of the  $\beta$ -tubulin tail is flexible within the active site of TTLL7 suggests that the active site of this  $\beta$ -tubulin-specific glutamylase has evolved to accommodate a range of  $\beta$ -tubulin tails of different lengths. This is particularly important for  $\beta$ -tubulin-modifying enzymes, as in contrast to  $\alpha$ -tubulin, the C-terminal tails of  $\beta$ -tubulin isotypes show a higher variability in length (Fig 5D). Plotting the binding modes of the  $\beta$ -tubulin tail along the first principal component axis reveals concerted movements of the structural elements of TTLL7 and the  $\beta$ -tubulin tail (Fig EV2B) and confirmed the higher flexibility of the C-terminal end of the  $\beta$ -tubulin tail as compared to that of the  $\alpha$ -tubulin tail in TTLL5 (Fig EV2A).

### Molecular components involved in the binding of the $\beta$ -tubulin tail to TTLL7

Similar to  $\alpha$ -tubulin, the C-terminal tails of  $\beta$ -tubulin are rich in acidic amino acid residues, which are mostly glutamates (Fig 5D). Not surprisingly, our simulations generated a model in which the  $\beta$ -tubulin tail is also anchored to the active site of TTLL7 through series of its glutamate residues (Fig 5C), which form salt-bridge

#### Figure 5. Docking of the $\beta$ -tubulin tail into TTLL7.

- A, B Molecular dynamics simulations of TTLL7 in the apo- (cyan) and the  $\beta$ 2-tubulin-tail-bound (pink) form. (A) Time evolution of RMSD values of backbone atoms from TTLL7. The RMSD changes were calculated with respect to the equilibrated structure from apo- and tail-bound simulations. (B) RMSF values of C $\alpha$  atoms comparing apo- and tail-bound simulations.
- C Predicted interactions between the C-terminal tail of  $\beta$ 2-tubulin and active-site residues of TTLL7. The  $\beta$ -tubulin tail is shown in pink and TTLL7 in cyan. The yellow dotted lines denote the hydrogen bonding interactions.
- D Sequence alignment of all C-terminal tails of  $\alpha$ - and  $\beta$ -tubulin [54]. The residues are colour-coded according to their type. Note that despite the greater diversity and length of  $\beta$ -tubulin tails, core interaction sites with TTLLs are similarly distributed in both  $\alpha$ - and  $\beta$ -tubulin tails.

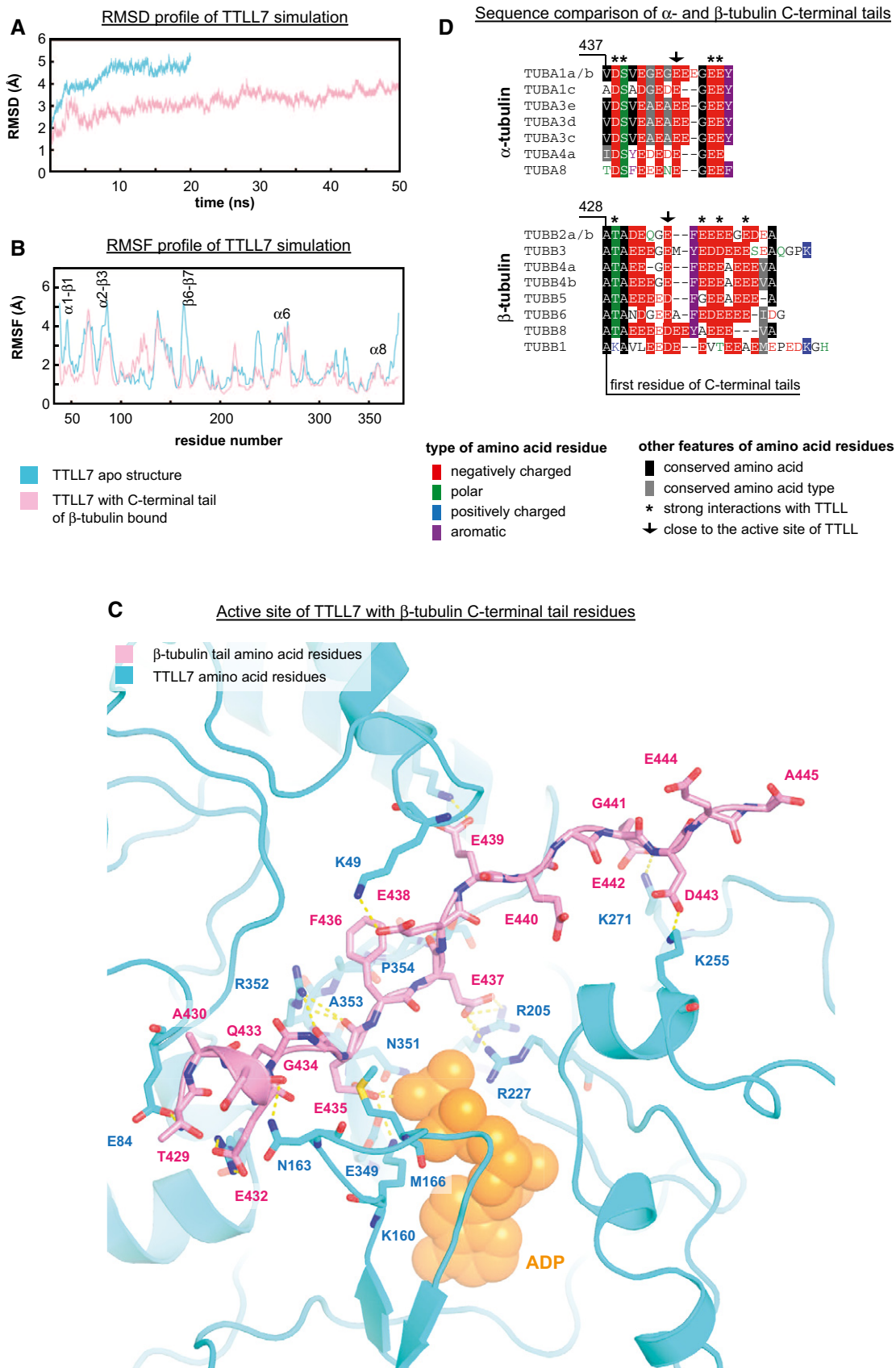


Figure 5.

interactions with the stretch of positive residues, K49, R205, R227, R250, K255, K271 and R352 of TLL7. Our predicted binding mode (Fig 5C) is consistent with a previous study in which mutations of the TLL7 residues R205, R227, K271 and R352 result in loss of enzymatic activity [13].

The residue E435 of the  $\beta$ 2-tubulin tail is located in close vicinity to ADP/ATP, suggesting that this residue could be preferentially modified by TLL7. In contrast to the  $\alpha$ -tubulin isoforms, most  $\beta$ -tubulin isoforms contain a unique aromatic residue in a conserved position (F436 in  $\beta$ 2-tubulin; Fig 5D). This unique residue makes hydrophobic contacts with residues A353 and the P354 of TLL7 (Fig 5C) and might thus favour the proximity of E435 to the nucleotide to initiate catalysis. Strikingly, A353 is substituted by a polar serine residue in TLL4, TLL5 and TLL6 (Fig EV1), which might weaken the hydrophobic interactions with F436. This could explain why specifically TLL7, but not TLL4, another  $\beta$ -tubulin glutamylase, shows a particularly stringent selectivity for modifying  $\beta$ -tubulin [7].

Our simulations strongly suggest that all glutamylases bind the C-terminal tubulin tails in a similar mode, which is mainly driven by electrostatic attraction. Indeed, the overlay of the modelled structures of TLL4, TLL5, TLL6 and TLL7 shows no change in the positioning of the key residues (Fig 6). However, there are two particularities of the binding of the  $\beta$ -tubulin tail to TLL7. First, recognition of the  $\beta$ -tubulin tail is mediated through docking of F436, a unique aromatic residue found in most  $\beta$ -tubulin tails, but absent from  $\alpha$ -tubulin tails (Fig 5D). This could confer specificity to  $\beta$ -tubulin-modifying glutamylases. Second, the very C-terminus of the  $\beta$ -tubulin tail projects out of the active site of

TLL7 in our model, making it appealing to speculate that the tails protrude from the active site of TLL7 without undergoing other structural interactions with the enzyme. As this binding mode allows for accommodating  $\beta$ -tubulin tails of disparate lengths, our observation indicates that TLL7 can potentially modify all isoforms of  $\beta$ -tubulin. This is functionally important, as the C-terminal tails of  $\beta$ -tubulins are more variable in length than  $\alpha$ -tubulin tails (Fig 5D). Coherently, our structural model of TLL5 has revealed a rather closed active site with a distinct binding site for the conserved tyrosine residue at the C-terminus of  $\alpha$ -tubulin.

## Discussion

Tubulin (poly)glutamylation and (poly)glycylation are important elements of the tubulin code. Both PTMs generate a large variety of biochemically distinct signals, and combinations of these signals at the MT lattice are expected to selectively control different MT functions (discussed in [2,22]). Characteristic patterns of glutamylation and glycylation have been found in cilia and flagella [23–25], centrosomes [26] and neurons [27,28], indicating that the generation of these patterns is strictly controlled in cells.

Recent studies have begun to shed light on the mechanisms of polyglutamylation. Initial *in vitro* studies using tubulin with differential polyglutamylation patterns demonstrated that not only the presence, but also the pattern of this modification plays a key role in regulating spastin-mediated MT severing [5,29]. Intriguingly, glutamylation works as a rheostat: it activates severing at an optimum modification level, and inhibits it when glutamylation is

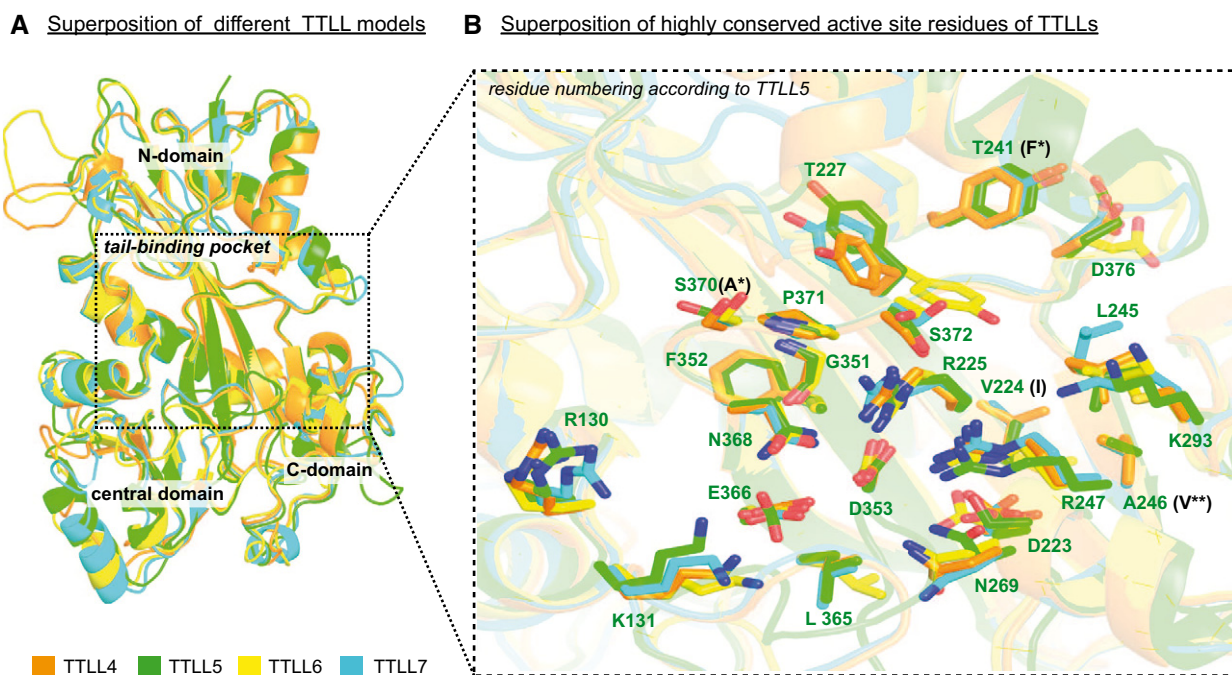


**Figure 6. Structural comparison of models for different glutamylase enzymes.**

A Superposition of structural models of the core domains of TLL4 (orange), TLL5 (green), TLL6 (yellow) and TLL7 (cyan).

B Detailed view of (A), with the highly conserved residues in the active site around 5-Å distances are represented in the stick representation. Note that most key residues of the active site are arranged nearly identically in all four polyglutamylases.

further accumulated [5]. Using chimeric recombinant tubulin with chemically added polyglutamylation showed a selective regulation of some kinesin motors by this PTM, and again, the length of the added glutamate chains played an important regulatory role [30]. These studies clearly underscore the importance of controlling the patterns of glutamylation in cells, raising questions about how these different patterns are generated, and how precisely are they controlled by the enzymatic machinery.

The identification of nine glutamylases within the TTL family [6,7,31] revealed that the glutamylation patterns are directly encoded in the enzymes; each TTL showed an enzymatic preference for modifying either  $\alpha$ - or  $\beta$ -tubulin and for generating short or long glutamate chains. However, when overexpressed in cells, most enzymes lost these preferences and modified both,  $\alpha$ - and  $\beta$ -tubulin [7]. Similar observations were also made for glycylation, for which only three enzymes exist in mammals [8,32,33]. Thus, TTL enzymes have preferences that allow them to write a particular PTM pattern on the MTs, but can also sidestep and generate different patterns, a process that could be controlled by either the levels of enzymes, the longevity of the MTs, or by other regulatory processes that control the enzymatic activity.

To decipher the code written by TTL enzymes, it is crucial to elucidate how these enzymes interact with their substrates—the C-terminal tails of tubulin. Because a structural study of the glutamylase could not visualize the entire tubulin tail in the active site of this enzyme [13], and no other structural data of glutamylases or glycylation are available, we used a computational approach combining molecular modelling, docking and dynamic simulations to visualize the binding modes of tubulin tails into the active sites of TTLs. In our models, the active sites of the TTLs show a high degree of plasticity, and undergo structural remodelling upon the docking of the C-terminal tail of tubulin. Our docking further provides a structural model for the experimentally determined major modification sites, E445 on  $\alpha$ 1-tubulin [3] and E435 on  $\beta$ 2-tubulin [34]: both residues are positioned in the close vicinity of the ATP/ADP-binding site. The high similarity of the binding mode of  $\alpha$ -tubulin tails to TTL5 and  $\beta$ -tubulin tails to TTL7 provides a rationale for the observation that most TTLs are able to modify both  $\alpha$ - and  $\beta$ -tubulin [7]. This confirms a model in which the binding of the entire enzyme to the MT surface, but not the specificity of the C-terminal tails to the active site, determines the specificity of a TTL to either  $\alpha$ - or  $\beta$ -tubulin [13]. As the outer surface of MTs is structurally very similar between the  $\alpha$ - and  $\beta$ -tubulin subunits, the TTLs might bind and modify both tubulins, though with different efficiencies. The only exception is TTL7, which is highly specific to  $\beta$ -tubulin [5,7]. Our model provides one possible explanation for this specificity: TTL7 is unique in having two hydrophobic interactions with an aromatic residue that in turn is unique to the  $\beta$ -tubulin tails (Fig 5D, phenylalanine 436 in  $\beta$ 2-tubulin).

Tubulin tails are highly flexible, undergoing structural changes to fit into the active-site environment, which favours an induced-fit model of enzyme dynamics (Fig EV2). This implies that most of the mammalian tubulin isoforms can be modified by these enzymes, first, because the key residues involved in the fitting of the tails into the active site are conserved in most isoforms (Fig 5D), and secondly because in our model, the tubulin tails are not fully stretched out when bound to the TTL active pocket, which would also allow to

accommodate isoforms with different lengths of C-terminal tails than those used for our simulations ( $\alpha$ 1/TUBA1;  $\beta$ 2/TUBB2; Fig 5D). A similar mechanism had been proposed for TTL [12].

Our results provide a theoretical framework that should guide further experimental work to validate its predictions. Nevertheless, our models advance the understanding of the molecular mechanisms that govern the generation of complex PTM patterns on MTs. This has important functional implications, as altered levels and patterns of glutamylation and glycylation have been reported in human diseases or disease models, such as cancer [35,36], neurodegeneration [10], ciliopathies [25,37,38] including male sperm dysfunctions [8,39–43] and retina degeneration [42,44,45].

Our work supports a model for the enzymatic mechanism of TTL enzymes in which the oriented binding of the enzymes to the MT lattice is the primary determinant for their selectivity for  $\alpha$ - or  $\beta$ -tubulin. In contrast, due to the high similarity of their active sites (Fig 6), most TTL enzymes are intrinsically compatible with the modification of both,  $\alpha$ - and  $\beta$ -tubulin tails. Our model now provides an intriguing perspective on how alterations of modification patterns on MTs could be achieved. For instance, a simple deregulation of mechanisms that localize TTL enzymes to MTs could lead not only to an over- or under-modification of the affected MTs, but, due to local changes in enzyme concentration and/or activity, induce changes of glutamylation and glycylation patterns. As distinct PTM patterns are likely to govern distinct MT functions, a loss of specificity in tubulin modification could thus have a strong functional impact, even without significantly affecting the overall PTM levels. Finally, our modelling studies will help designing effective drugs against TTL enzymes, which could have an important impact on the development of novel therapies related to the emerging role of glutamylation and glycylation in human diseases.

## Materials and Methods

Detailed experimental procedures for molecular modelling, molecular dynamics simulations and mutagenesis are in Methods EV1.

### Molecular modelling

The TTL core domains of TTL4, TTL5, TTL6 and TTL7 were homology-modelled using modeller 9v7 [46] based on the X-ray crystal structures of TTL7 (PDB 4YLR) and TTL (PDB 4I4T), further refined with GalaxyRefine [47] web server and checked with a Ramachandran plot. The models were further energy-minimized to avoid any steric clashes.

The full-length  $\alpha$ - and  $\beta$ -tubulin dimer was modelled from the structure PDB 4I4T [12], and the C-terminal tail sequences were truncated ( $\alpha$ -tubulin tail: residues 438–451;  $\beta$ -tubulin tail: residues 429–445) and docked into the active sites of TTL5 and TTL7, respectively.

Structure files are available in Model EV1 and can be viewed with an appropriate software for pdb files: TTL4\_model.pdb (modelled structure of the catalytic core domain of murine TTL4; Figs 1, 4B and 6); TTL5\_model.pdb (modelled structure of the catalytic core domain of murine TTL5; Figs 1, 4B and 6); TTL6\_model.pdb (modelled structure of the catalytic core domain of murine TTL6;

Figs 1, 4B and 6); TLL7\_model.pdb (modelled structure of the catalytic core domain of murine TLL7; Figs 1, 4B and 6).

### MD simulations

TLL5 and TLL7 were simulated using CHARMM C36FF [48] force field with NAMD 2.10 [49] package, either without (apo-forms) or with the tubulin tails. Simulations were performed under periodic boundary conditions, and the models were solvated in an octahedral box of explicit water molecules. The models were energy-minimized without restraints for 10,000 steps and then gradually equilibrated over 9 ns. Finally, the simulations were continued for 50 ns. RMSD values were calculated for each frame along the entire trajectory as a function of time, with respect to the equilibrated starting structures from TLL5 or TLL7 simulations. The C $\alpha$  RMSF were calculated to detect the average fluctuations of each residue during simulations. Principal component analysis (PCA) was performed using GROMACS package [50]. The hydrogen bond analysis was performed through H-bond plug-in in VMD [16]. Structure files are available in Model EV1 and can be viewed with an appropriate software for pdb files: TLL5\_subs\_50 ns.pdb (structure of the catalytic core domain of murine TLL5 with the C-terminal tail of  $\alpha$ 1-tubulin [TubA1A, amino acids 438–451] after 50 ns of molecular dynamics simulations; Figs 2, 3A and 4A, Methods EV1); TLL7\_subs\_50 ns.pdb (structure of the catalytic core domain of murine TLL7 with the C-terminal tail of  $\beta$ 2-tubulin [TubB2B; amino acids 429–445] after 50 ns of molecular dynamics simulations; Fig 5C; Methods EV1).

### Site-directed mutagenesis of TLL5

Polymerase chain reactions with two mutagenic primer pairs (Methods EV1) were performed using the Kapa-Hifi polymerase (Kapa Biosystems) and 16 cycles of amplification. To delete or replace the  $\beta$ 6- $\beta$ 7 loop of TLL5, pEYFP-spacer-mTLL5 [7] was amplified with specific primers (Methods EV1), circularized using a ligation-independent method [19] Single colonies were picked and plasmid DNA was verified by sequencing.

### Cell culture and transfection

HEK293T (human embryonic kidney) cells were cultured on plastic dishes under standard conditions, using DMEM culture media (Thermo Fisher Scientific) containing 10% FBS (Sigma-Aldrich). Transfection of expression plasmids was carried out in JetPei (Polyplus) transfection medium, according to the manufacturer's instructions. 20 h after transfection, cells were either directly lysed in Laemmli buffer for immunoblot analyses, or, for activity assays, detached with PBS+0.5 mM EDTA, pelleted at 100 g and lysed in ice-cold 40  $\mu$ l MEM buffer (50 mM Mes/NaOH, pH 6.8; 2 mM EGTA; 1 mM MgCl<sub>2</sub>) containing 0.2% NP-40 and protease inhibitors for 10 min. Clear supernatants were collected for *in vitro* assays.

### Immunoblot analyses

The cell lysate in Laemmli buffer was resolved either in 8 or 10% polyacrylamide gels, transferred onto nitrocellulose membranes

(Trans-Blot<sup>®</sup> Turbo<sup>™</sup> Transfer System, BioRad) and subjected to immunoblot analysis with the following antibodies: mouse GT335 (Adipogen AG-20B-0020 1:2,000), rabbit polyE (Adipogen AG-25B-0030 1:8,000), mouse 12G10 (University of Iowa Developmental Studies Hybridoma Bank 1:500) and rabbit anti-TLL5 serum (1:2,000) for 2 h at room temperature. The membranes were incubated with goat anti-rabbit or anti-mouse secondary antibodies conjugated to horseradish peroxidase (1:10,000, HRP; GE Healthcare) and developed using ECL Western blotting detection reagent (GE Healthcare).

### *In vitro* polyglutamylase assay

The enzymatic activity of TLL5 was directly assessed from the extracts of HEK293T cells overexpressing the different TLL5-YFP constructs as described earlier [6,51]. Briefly, 20- $\mu$ l reaction mixtures contained 4  $\mu$ l of cell lysate, 4  $\mu$ l [<sup>3</sup>H]-glutamate (40–80 Ci/mmol; Perkin Elmer) and 0.2 mg/ml of polymerized, Taxotere-stabilized pork brain MTs in MQ reaction buffer (50 mM Tris-HCl, pH 9.0; 500  $\mu$ M DTT; 4  $\mu$ M Taxotere; 2.4 mM MgCl<sub>2</sub>; 400  $\mu$ M ATP). The reactions were incubated for 2 h at 37°C, and stopped by boiling with Laemmli buffer. The samples were run on 10% SDS-PAGE gels to separate  $\alpha$ - and  $\beta$ -tubulin bands [20], transferred onto a nitrocellulose membrane and stained with Ponceau S in 1% acetic acid. The individual  $\alpha$ - and  $\beta$ -tubulin bands were cut out, dissolved in scintillation liquid (Filter-Count-LSC; Perkin Elmer), and [<sup>3</sup>H]-glutamate incorporation was measured in a scintillation counter (Tri-Carb 2910 TR with QuantaSmart v4.00; Perkin Elmer) as described before [6]. The mean values and standard deviation of three individual experiments were plotted separately for  $\alpha$ - and  $\beta$ -tubulin as graphs of total [<sup>3</sup>H]-glutamate incorporation [dpm] versus the sample identity.

**Expanded View** for this article is available online.

### Acknowledgements

This work has received support under the programme “Investissements d’Avenir” launched by the French Government and implemented by ANR with the references ANR-10-LBX-0038, ANR-10-IDEX-0001-02 PSL\*. The work was further supported by the grants ANR-12-BSV2-0007, INCA 2013-1-PLBIO-02-ICR-1 and 2014-PLBIO-11-ICR-1. KN is supported by the FRM fellowship SPF20140129173, JS by the FRM fellowship SPF20120523942, and the EMBO ALTF 638-2010 and EMBO ASTF 445-2012. We would like to thank L. Mouawad and E. Quiniou (Institut Curie, INSERM U759) for providing us computational server access for the simulations. The antibody 12G10 developed by J. Frankel and M. Nelson was obtained from the Developmental Studies Hybridoma Bank developed under the auspices of the NICHD and maintained by the University of Iowa. We are grateful to M. Steinmetz (PSI, Villigen, Switzerland), S. Haibin (Nanyang Technological University, Singapore), M. Zacharias (Technical University Munich, Germany), S. Bodakuntla and P. Singh for critical reading of the manuscript.

### Author contributions

Conceptualization: KN, JS, CJ; Methodology: KN, MMM, CJ; Software: KN; Validation: KN, SG; Formal analysis: KN, SG; Investigation: KN, SG, CJ; Writing—original draft: KN, CJ; Writing—review & editing: KN, SG, MMM, CJ; Visualization: KN, CJ; Supervision: CJ; Project administration: CJ; Funding acquisition: KN, JS, CJ.

## Conflict of interest

The authors declare that they have no conflict of interest.

## References

- Chakraborti S, Natarajan K, Curiel J, Janke C, Liu J (2016) The emerging role of the tubulin code: from the tubulin molecule to neuronal function and disease. *Cytoskeleton* 73: 521–550
- Janke C (2014) The tubulin code: molecular components, readout mechanisms, and functions. *J Cell Biol* 206: 461–472
- Eddé B, Rossier J, Le Caer JP, Desbruyeres E, Gros F, Denoulet P (1990) Posttranslational glutamylation of alpha-tubulin. *Science* 247: 83–85
- Redeker V, Levilliers N, Schmitter JM, Le Caer JP, Rossier J, Adoutte A, Bré MH (1994) Polyglycylation of tubulin: a posttranslational modification in axonemal microtubules. *Science* 266: 1688–1691
- Valenstein ML, Roll-Mecak A (2016) Graded control of microtubule severing by tubulin glutamylation. *Cell* 164: 911–921
- Janke C, Rogowski K, Wloga D, Regnard C, Kajava AV, Strub J-M, Temurak N, van Dijk J, Boucher D, van Dorsselaer A et al (2005) Tubulin polyglutamylase enzymes are members of the TTL domain protein family. *Science* 308: 1758–1762
- van Dijk J, Rogowski K, Miro J, Lacroix B, Eddé B, Janke C (2007) A targeted multienzyme mechanism for selective microtubule polyglutamylase. *Mol Cell* 26: 437–448
- Rogowski K, Juge F, van Dijk J, Wloga D, Strub J-M, Levilliers N, Thomas D, Bré MH, Van Dorsselaer A, Gaertig J et al (2009) Evolutionary divergence of enzymatic mechanisms for posttranslational polyglycylation. *Cell* 137: 1076–1087
- Wloga D, Webster DM, Rogowski K, Bré MH, Levilliers N, Jerka-Dziadosz M, Janke C, Dougan ST, Gaertig J (2009) TTL3 is a tubulin glycine ligase that regulates the assembly of cilia. *Dev Cell* 16: 867–876
- Rogowski K, van Dijk J, Magiera MM, Bosc C, Deloulme J-C, Bosson A, Peris L, Gold ND, Lacroix B, Bosch Grau M et al (2010) A family of protein-deglutamylating enzymes associated with neurodegeneration. *Cell* 143: 564–578
- Ersfeld K, Wehland J, Plessmann U, Dodemont H, Gerke V, Weber K (1993) Characterization of the tubulin-tyrosine ligase. *J Cell Biol* 120: 725–732
- Prota AE, Magiera MM, Kujpers M, Bargsten K, Frey D, Wieser M, Jaussi R, Hoogenraad CC, Kammerer RA, Janke C et al (2013) Structural basis of tubulin tyrosination by tubulin tyrosine ligase. *J Cell Biol* 200: 259–270
- Garnham CP, Vemu A, Wilson-Kubalek EM, Yu I, Szyk A, Lander GC, Milligan RA, Roll-Mecak A (2015) Multivalent microtubule recognition by tubulin tyrosine ligase-like family glutamylases. *Cell* 161: 1112–1123
- Luchko T, Huzil JT, Stepanova M, Tuszyński J (2008) Conformational analysis of the carboxy-terminal tails of human beta-tubulin isoforms. *Biophys J* 94: 1971–1982
- Szyk A, Deaconescu AM, Piszczek G, Roll-Mecak A (2011) Tubulin tyrosine ligase structure reveals adaptation of an ancient fold to bind and modify tubulin. *Nat Struct Mol Biol* 18: 1250–1258
- Humphrey W, Dalke A, Schulten K (1996) VMD: visual molecular dynamics. *J Mol Graph* 14: 33–38
- Camacho CJ, Zhang C (2005) FastContact: rapid estimate of contact and binding free energies. *Bioinformatics* 21: 2534–2536
- Zhang C, Vasmatzis G, Cornette JL, DeLisi C (1997) Determination of atomic desolvation energies from the structures of crystallized proteins. *J Mol Biol* 267: 707–726
- Jeong J-Y, Yim H-S, Ryu J-Y, Lee HS, Lee J-H, Seen D-S, Kang SG (2012) One-step sequence- and ligation-independent cloning as a rapid and versatile cloning method for functional genomics studies. *Appl Environ Microbiol* 78: 5440–5443
- Magiera MM, Janke C (2013) Investigating tubulin posttranslational modifications with specific antibodies. *Journal* 115: 247–267
- van Dijk J, Miro J, Strub J-M, Lacroix B, van Dorsselaer A, Eddé B, Janke C (2008) Polyglutamylase is a post-translational modification with a broad range of substrates. *J Biol Chem* 283: 3915–3922
- Roll-Mecak A (2015) Intrinsically disordered tubulin tails: complex tuners of microtubule functions? *Semin Cell Dev Biol* 37C: 11–19
- Gagnon C, White D, Cosson J, Huitorel P, Eddé B, Desbruyeres E, Paturle-Lafanechere L, Multigner L, Job D, Cibert C (1996) The polyglutamylated lateral chain of alpha-tubulin plays a key role in flagellar motility. *J Cell Sci* 109: 1545–1553
- Million K, Larcher J, Laoukili J, Bourguignon D, Marano F, Tournier F (1999) Polyglutamylase and polyglycylation of alpha- and beta-tubulins during *in vitro* ciliated cell differentiation of human respiratory epithelial cells. *J Cell Sci* 112: 4357–4366
- Bosch Grau M, Gonzalez Curto G, Rocha C, Magiera MM, Marques Sousa P, Giordano T, Spassky N, Janke C (2013) Tubulin glycylation and glutamylases have distinct functions in stabilization and motility of ependymal cilia. *J Cell Biol* 202: 441–451
- Bobinnec Y, Moudjou M, Fouquet JP, Desbruyeres E, Eddé B, Bornens M (1998) Glutamylase of centriole and cytoplasmic tubulin in proliferating non-neuronal cells. *Cell Motil Cytoskeleton* 39: 223–232
- Audebert S, Koulakoff A, Berwald-Netter Y, Gros F, Denoulet P, Eddé B (1994) Developmental regulation of polyglutamylated alpha- and beta-tubulin in mouse brain neurons. *J Cell Sci* 107: 2313–2322
- Audebert S, Desbruyeres E, Gruszczynski C, Koulakoff A, Gros F, Denoulet P, Eddé B (1993) Reversible polyglutamylase of alpha- and beta-tubulin and microtubule dynamics in mouse brain neurons. *Mol Biol Cell* 4: 615–626
- Lacroix B, van Dijk J, Gold ND, Guizetti J, Aldrian-Herrada G, Rogowski K, Gerlich DW, Janke C (2010) Tubulin polyglutamylase stimulates spastin-mediated microtubule severing. *J Cell Biol* 189: 945–954
- Sirajuddin M, Rice LM, Vale RD (2014) Regulation of microtubule motors by tubulin isoforms and post-translational modifications. *Nat Cell Biol* 16: 335–344
- Ikegami K, Mukai M, Tsuchida J-I, Heier RL, Macgregor GR, Setou M (2006) TTL7 is a mammalian beta-tubulin polyglutamylase required for growth of MAP2-positive neurites. *J Biol Chem* 281: 30707–30716
- Wloga D, Rogowski K, Sharma N, Van Dijk J, Janke C, Edde B, Bré MH, Levilliers N, Redeker V, Duan J et al (2008) Glutamylase on alpha-tubulin is not essential but affects the assembly and functions of a subset of microtubules in *Tetrahymena thermophila*. *Eukaryot Cell* 7: 1362–1372
- Ikegami K, Setou M (2009) TTL10 can perform tubulin glycylation when co-expressed with TTL8. *FEBS Lett* 583: 1957–1963
- Rüdiger M, Plessman U, Kloppel KD, Wehland J, Weber K (1992) Class II tubulin, the major brain beta tubulin isoform is polyglutamylated on glutamic acid residue 435. *FEBS Lett* 308: 101–105
- Souček K, Kamaid A, Phung AD, Kubala L, Bulinski JC, Harper RW, Eiserich JP (2006) Normal and prostate cancer cells display distinct molecular profiles of alpha-tubulin posttranslational modifications. *Prostate* 66: 954–965
- Rocha C, Papon L, Cacheux W, Marques Sousa P, Lascano V, Tort O, Giordano T, Vacher S, Lemmers B, Mariani P et al (2014) Tubulin

- glycylases are required for primary cilia, control of cell proliferation and tumor development in colon. *EMBO J* 33: 2247–2260
37. Lee JE, Silhavy JL, Zaki MS, Schroth J, Bielas SL, Marsh SE, Olvera J, Brancati F, Iannicelli M, Ikegami K et al (2012) CEP41 is mutated in Joubert syndrome and is required for tubulin glutamylation at the cilium. *Nat Genet* 44: 193–199
  38. Pathak N, Austin CA, Drummond IA (2011) Tubulin tyrosine ligase-like genes *tll3* and *tll6* maintain Zebrafish cilia structure and motility. *J Biol Chem* 286: 11685–11695
  39. Lee G-S, He Y, Dougherty EJ, Jimenez-Movilla M, Avella M, Grullon S, Sharlin DS, Guo C, Blackford JA, Awasthi S et al (2013) Disruption of *Tll5/Stamp* gene (Tubulin tyrosine ligase-like protein 5/SRC-1 and TIF2 associated modulatory protein gene) in male mice causes sperm malformation and infertility. *J Biol Chem* 288: 15167–15180
  40. Vogel P, Hansen G, Fontenot G, Read R (2010) Tubulin tyrosine ligase-like 1 deficiency results in chronic rhinosinusitis and abnormal development of spermatid flagella in mice. *Vet Pathol* 47: 703–712
  41. Ikegami K, Sato S, Nakamura K, Ostrowski LE, Setou M (2010) Tubulin polyglutamylation is essential for airway ciliary function through the regulation of beating asymmetry. *Proc Natl Acad Sci USA* 107: 10490–10495
  42. Bedoni N, Haer-Wigman L, Vaclavik V, Tran HV, Farinelli P, Balzano S, Royer-Bertrand B, El-Asrag ME, Bonny O, Ikonomidis C et al (2016) Mutations in the polyglutamylase gene *TLL5*, expressed in photoreceptor cells and spermatozoa, are associated with cone-rod degeneration and reduced male fertility. *Hum Mol Genet* 25: 4546–4555
  43. Konno A, Ikegami K, Konishi Y, Yang H-J, Abe M, Yamazaki M, Sakimura K, Yao I, Shiba K, Inaba K et al (2016) *Tll9*<sup>-/-</sup> mice sperm flagella show shortening of doublet 7, reduction of doublet 5 polyglutamylation and a stall in beating. *J Cell Sci* 129: 2757–2766
  44. Blanks JC, Spee C (1992) Retinal degeneration in the *pcd/pcd* mutant mouse: accumulation of spherules in the interphotoreceptor space. *Exp Eye Res* 54: 637–644
  45. Bosch Grau M, Masson C, Gadadhar S, Rocha C, Tort O, Sousa PM, Vacher S, Bieche I, Janke C (2017) Alterations in the balance of tubulin glycylation and glutamylation in photoreceptors leads to retinal degeneration. *J Cell Sci* 130: 938–949
  46. Sali A, Blundell TL (1993) Comparative protein modelling by satisfaction of spatial restraints. *J Mol Biol* 234: 779–815
  47. Heo L, Park H, Seok C (2013) GalaxyRefine: protein structure refinement driven by side-chain repacking. *Nucleic Acids Res* 41: W384–W388
  48. Best RB, Zhu X, Shim J, Lopes PEM, Mittal J, Feig M, Mackerell AD Jr (2012) Optimization of the additive CHARMM all-atom protein force field targeting improved sampling of the backbone phi, psi and side-chain chi(1) and chi(2) dihedral angles. *J Chem Theory Comput* 8: 3257–3273
  49. Phillips JC, Braun R, Wang W, Gumbart J, Tajkhorshid E, Villa E, Chipot C, Skeel RD, Kale L, Schulten K (2005) Scalable molecular dynamics with NAMD. *J Comput Chem* 26: 1781–1802
  50. Hess B, Kutzner C, van der Spoel D, Lindahl E (2008) GROMACS 4: algorithms for highly efficient, load-balanced, and scalable molecular simulation. *J Chem Theory Comput* 4: 435–447
  51. Regnard C, Audebert S, Desbruyeres Denoulet P, Eddé B (1998) Tubulin polyglutamylase: partial purification and enzymatic properties. *Biochemistry* 37: 8395–8404
  52. Ashkenazy H, Abadi S, Martz E, Chay O, Mayrose I, Pupko T, Ben-Tal N (2016) ConSurf 2016: an improved methodology to estimate and visualize evolutionary conservation in macromolecules. *Nucleic Acids Res* 44: W344–W350
  53. Dosztányi Z, Mészáros B, Simon I (2009) ANCHOR: web server for predicting protein binding regions in disordered proteins. *Bioinformatics* 25: 2745–2746
  54. Chenna R, Sugawara H, Koike T, Lopez R, Gibson TJ, Higgins DG, Thompson JD (2003) Multiple sequence alignment with the Clustal series of programs. *Nucleic Acids Res* 31: 3497–3500
  55. Pettersen EF, Goddard TD, Huang CC, Couch GS, Greenblatt DM, Meng EC, Ferrin TE (2004) UCSF Chimera—a visualization system for exploratory research and analysis. *J Comput Chem* 25: 1605–1612